Scaling-up the use of macroscopic photo-CWPO La1-xTixFeO3/SiC alveolar foam catalyst for solar water treatment against micropollutants

Patricia García-Muñoz, Aimé Abega, Alba Hernández-Zanoletty, Didier Robert, Sixto Malato, Nicolas Keller

Scaling-up the use of macroscopic photo-CWPO $La_{1-x}Ti_xFeO_3$/SiC alveolar foam catalyst for solar water treatment against micropollutants

Patricia García-Muñoz,[1*] Aimé Abega, [2] Alba Hernández-Zanoletty, [3] Didier Robert [2], Sixto Malato,[3] Nicolas Keller[2]

[1] Department of Chemical and Environmental Engineering, Escuela Técnica Superior de Ingenieros Industriales, Universidad Politécnica de Madrid, 28006 Madrid, Spain

[2] Institut de Chimie et Procédés pour l'Energie, l'Environnement et la Santé (ICPEES), CNRS/University of Strasbourg, 25 rue Becquerel, Strasbourg, France

[3] Plataforma Solar de Almería-CIEMAT, Ctra Senes km 4, Tabernas (Almería) 04200, Spain

*Corresponding authors: patricia.gmunoz@upm.es ; nkeller@unistra.fr

GRAPHICAL ABSTRACT

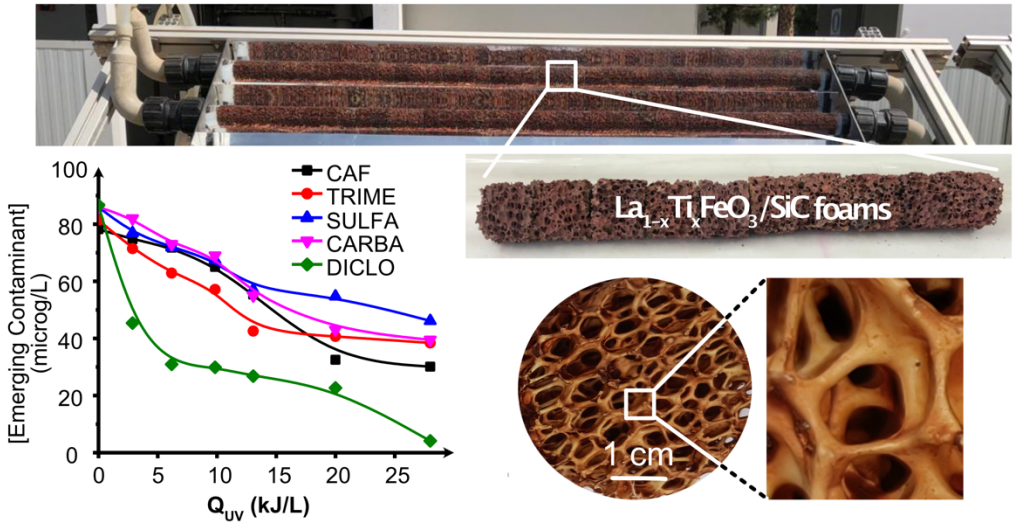

ABSTRACT

Current wastewater treatment plants are not prepared for the removal of micropollutants like phenol, pharmaceuticals and pesticides in water. As their release into the environment has adverse consequences towards the living organisms of ecosystems, the engineering of novel sustainable processes able to ultimately remove the emerging organic contaminants is an objective of paramount importance. Hereby we report for the first time on the successful scale-up of a macroscopic photo-CWPO $La_{1-x}Ti_xFeO_3$/SiC alveolar foam catalyst used at the pilot-plant scale inside a Compound Parabolic Collectors based photoreactor. The removal of a span of organic micropollutants in water matrices of different complexity was efficiently realized under natural solar radiation using H_2O_2 or persulfates as oxidizing agent. The water matrix composition affected the efficiency of the degradation process. Using H_2O_2, for a collected energy of *ca.* 27 KJ/mol, the rate of micropollutant removal ranged from 53% to 95% in distilled water depending on the micropollutant in a cocktail configuration. It was lowered to the 17-66% range in tap water, and to the 8-42% range in simulated urban wastewater. The results demonstrated the promise of using sodium persulfate as oxidant instead of H_2O_2, with a better efficiency towards the removal of most of the micropollutants tested. The use of the sodium persulfate oxidant allows for overcoming the drawbacks associated to the treatment of real water matrices observed using H_2O_2, as better performances were reached when increasing the water matrix complexity. Complete removal of carbamazepine and diclofenac micropollutants was reached in tap water and simulated urban wastewater for *ca.* 27 KJ/mol of collected energy. The degradation performances combined to the catalyst robustness make this water treatment technology promising for operating in a continuous way under natural solar light.

KEYWORDS:

Macroscopic photo-CWPO catalyst, $La_{1-x}Ti_xFeO_3$/SiC alveolar foam**,** wastewater treatment, micropollutants, process scale-up

1- INTRODUCTION

The presence of micropollutants such as phenol, pharmaceuticals and pesticides in the environment is due to their release from the human activities [1]. Due to the harmful effect they can have on the environment, the micropollutants are regulated by discharge limits. In some cases, they have been included into the priority pollutants list [2], the regulations being regularly actualized by successive EU decisions as 2015/495/UE, 2018/840/UE and 2020/1161/UE.

The current wastewater treatments are not engineered for an efficient removal of those contaminants, so that the development of novel sustainable processes efficient for the removal of those refractory pollutants is still an overarching objective. In this scenario, a wide span of Advanced Oxidation Processes (AOPs) is investigated as alternative or complement to the processes in place [3, 4]. Among them, the Fenton process and its heterogeneous Catalytic Wet Peroxide Oxidation (CWPO) analogue that both operate through the decomposition of H_2O_2 by Fe catalyst, as well as heterogeneous photocatalysis that is based on the activation of a semiconductor by photons of suitable wavelengths, have gained particular attention due to high efficiency and relatively low cost.

Recently, we demonstrated the capability of a robust single-phase nanoparticulate $La_{1-x}Ti_xFeO_3$ orthoferrite material to behave as a dual light-driven catalyst able to take advantage of a synergistic effect between heterogeneous photo-CWPO catalysis and photocatalysis [5, 6].

It generates HO_x° radicals by Fe-catalyzed H_2O_2 decomposition under light (photo-CWPO), while simultaneously showing photocatalytic activity thanks to its semiconductor nature with a suitable band gap and well-located electronic bands. The selective cationic substitution was shown to boost the sunlight-driven activity of the catalysts compared to the bare titanium-free $LaFeO_3$, owing to an enhanced photo-CWPO/photocatalysis synergy, an enhanced photogenerated charge carriers availability at the surface, and an electronic enrichment of the surface Fe species. It also boosted the catalyst robustness, so that the optimized $La_{1-x}Ti_xFeO_3$ catalyst with x=0.11 reached full mineralization of different refractory targets with improved degradation and mineralization rates, with no leaching of Fe to the solution and no loss of activity after many cycles. While most of the activity resulted from the photo-CWPO catalysis, photocatalysis was proposed to allow the cleaning of the catalyst surface from poisoning Fe-carboxylate complex intermediates that are blocking the mineralization and leading to Fe leaching to water [5, 7].

Up to now, most of the works on light-driven AOPs has been extensively conducted on powdery nanoparticulate catalysts. They require however the recurrent implementation of costly and time-consuming (nano)filtration recovery steps for separating/recovering the catalysts from the solution, what lowers irretrievably the viability of the remediation process [8, 9]. By contrast, although it might allow the water treatment processes to operate in a continuous mode, by far less works report on the application of heterogeneous light-driven AOP catalysts immobilized on macroscopic supports, due to inherent limitations resulting from a poor light distribution within the photoreactor core, a reduction of the exposed surface area or increased pressure drops [10-13]. The scale-up of heterogeneous processes for real applications has been less investigated than laboratory systems. Indeed, it requires the restricting engineering of non-powdery supports with a macrostructure allowing for the

processing of high flow rates at a low pressure drop while maintaining a high contact statistics between the pollutants and the surfaces, and a suitable light transmission to the reactor core. Additionally, the selected supports must be able to adapt to the photoreactor configuration, and must be of a chemical nature allowing for the robust and long-lasting immobilization of the photocatalyst in order to prevent from any detachment and leaching of the nanoparticles to the solution [10].

Among a span of macroscopic supports including notably the multi-channel metallic or ceramic materials [12-14], open-cell alveolar solid foams have attracted significant interest for immobilizing photocatalysts, because they provide a good compromise between antinomic features inherent to open and close structure systems [10, 15, 16]. Their ability to act as static mixer is also a worthy feature. Although Ni metallic foams are of interest, they suffer from low thermal resistance that avoids thermal treatment to fix durably the photocatalysts as well as from high costs [17]. Thus, low cost ceramic foams based on alumina or SiC remain open-cell structures of choice due to their higher mechanical and thermal resistance compared to polymer or carbon foams [18-20]. The reader can refer to [10] and [15] for more details.

In preliminary works, we evidenced that open-cell alveolar solid foams made of SiC were macroscopic structured supports of choice for immobilizing sol-gel TiO_2 and commercial TiO_2 P25 photocatalysts with application in the removal of a series of pesticides or nanoplastics in an continuous operation mode [11-15, 21]. Compared to photocatalysis, by far less works have reported on the use of alveolar foams - and in particular SiC foams - as support for Fenton-type catalysts. Magnetite powder, $BiFeO_3$, ferrisilicate or Fe-ZSM-5 have been immobilised on Ni or SiC foams and used as dark-Fenton foam catalysts for CWPO [22-25]. Recently photo-Fenton-like degradation was achieved under UV-A light on perovskite-type catalysts supported on

cordierite monoliths [26] and on TiO_2−$FeSO_4$ immobilised on metallic foams [27]. No data on TOC conversion or stability aspects were provided.

A preliminary lab-scale step forward toward a viable application of the $La_{1-x}Ti_xFeO_3$ catalyst material was recently achieved, with its immobilization on macroscopic open-cell alveolar SiC foams [28]. In a similar way than its powdery counterpart, the $La_{1-x}Ti_xFeO_3$/SiC foam catalyst combined photocatalytic and H_2O_2-mediated photo-CWPO activity under UV-A light. Substantial mineralization rates and high TOC conversions were achieved at circumneutral pH with 4-chlorophenol as model contaminant, and without any Fe release to the solution. It has also the advantage of being able to be manufactured with a cylindrical shape, compatible with tubular photoreactors.

Herein, we aim at assessing for the first time the implementation at the pilot-plant scale of the photo-CWPO $La_{1-x}Ti_xFeO_3$/SiC foam catalyst inside a photoreactor based on Compound Parabolic Collectors (CPC) operating under natural solar radiation. The removal of different organic micropollutants in wastewater matrices differing in terms of complexity using H_2O_2 or persulfates as oxidizing agent was accomplished.

2- MATERIALS AND METHODS

2.1- Water matrices and characterization

Three water matrices differing in terms of composition and complexity were used to evaluate the performance of the catalyst on the pilot scale, namely, i) deionized water (DW), ii) real tap water (TW) and iii) simulated urban secondary wastewater effluent (SUWW). The Total Organic Carbon (TOC) and the inorganic anions or cations were measured with a Shimadzu 138 TOC-VCN analyzer and a Metrohm ionic chromatograph Model 850, respectively. The initial pH

values of DW and TW were 5.8 ± 0.1 and 6.5 ± 0.1. The ionic composition of TW is shown in Table 1.

Simulated urban wastewater was prepared from distilled water by addition of the different compounds listed in Table 2. After overnight stirring, the pH value of SUWW was 7.7 ± 0.1.

Table 1. Ionic composition of tap water (TW).

Compound	**mg/L**
F^-	0.3
Cl^-	334
Br^-	3.4
NO_3^-	11
SO_4^{2-}	109
$C_2O_4^{2-}$	1.1
NO_2^-	-
Na^+	217
NH_4^+	-
K^+	2.8
Mg^{2+}	31

Table 2. Composition of the simulated urban wastewater (SUWW).

Compounds	**mg/L**
$NaHCO_3$	96
$MgSO_4$	60
NaCl	580
KH_2PO_4	7
$CaSO_4,2H_2O$	60
$(NH_4)_2SO_4$	23.6
KCl	4
Beef extract	1.8
Peptone	2.7
Humic acid	4.2
Sodium lignin	2.4
Sodium lamyl sulfate	0.9
Tannic acid	4.2
Aracia gum powder	4.7

2.2- Reagents

4-Chlorophenol (4-CP) was used as model contaminant at a concentration of 20 mg/L. The pH values of the starting 4-CP solutions were 5.5, 6.3 and 7.2 in DW, TP and SUWW, respectively. Imidacloprid (IMI) was used as model micropollutant at 1000 µg/L. A mix of different micropollutants (MPs), namely Caffeine (CAF), Trimethoprim (TRIME), Sulfamethoxazole (SULFA), Carbamazepine (CARBA) and Diclofenac (DICLO), was also used, at an initial concentration of 100 µg/L. The micropollutants were added to the pilot plant from a methanolic stock solution with 2.5 g/L of each compound for allowing the complete subsequent dissolution of the micropollutants in 10 L of water, what consequently added only a few mg/L of extra TOC to the water matrix.

2.3- Catalyst preparation

SiC alveolar foams with 10 PPI were purchased from Nanning Elaiter Environmental Technologies Co. Ltd (China). They are mainly composed at *ca.* 80% of multiple SiC polytypes, notably α (4H and 6H) and β (3C), and at *ca.* 20% of alumina. They were used in this study as 46 mm (d) x 36 mm (h) cylinders. Prior to the ferrite synthesis, the foams were calcined at 1000°C to remove by combustion potential carbon residues from synthesis process, and to form a natural washcoat made of amorphous oxygenated phases at the foam surface favouring the *in situ* synthesis of the ferrite on the foam.

The Ti-modified $LaFeO_3$/SiC alveolar foam catalysts were elaborated according to the synthesis protocol described in García-Muñoz et al. [28]. They were prepared by dropwise incipient wetness impregnation of the SiC foam disks, by implementing a sol−gel citric acid based Pechini synthesis in the presence of dried amorphous sol−gel titania as a titanium source,

with final calcination at 800°C for 2 h. Synthesis details can be found in [28].

2.4- Analysis techniques

The concentration of Imidacloprid and MPs in the mix was followed by ultra-performance liquid chromatography (UPLC) (Agilent Technologies, Series 1200) with a UV-DAD detector at 273 nm and a C-18 analytical column (ZORBAX Eclipse XDB-C18, 600 bar, 1.8 µm, 4.6 x 50 mm). For imidacloprid, 5% of ACN as mobile phase A and 95% ultrapure water with 25 mM of formic acid as mobile phase B were used applying a gradient from 5 to 100% of A during 13 min, with a re-equilibrium time of 3 min. It was detected at 273 nm. For MPs in the mix, the mobile phases A and B described above were used. A linear progressive gradient from 5% to 80% of A was used until 13 min and then to 100% for 1 min. Caffeine, Trimethoprim, Sulfamethoxazole, Carbamazepine and Diclofenac were determined at 270, 270, 267, 267 and 285 nm, respectively. The injection volume was 50 µL and the flow rate 1 mL/min.

The concentration of 4-CP was followed by high-performance liquid chromatography (HPLC) (Agilent Technologies, Series 1100) with a UV-DAD detector at 228 nm and a C-18 analytical column (Luna C18, 150 × 3 mm, 100 Å, 5 µm, purchased from Phenomenex, Torrance, CA, USA). It was analyzed with 25 mM formic acid (40%) and methanol (60%) as mobile phase at 228 nm. The injection volume was 20 µL and the flow rate 0.5 mL/min.

The concentration of the dissolved iron was measured at the end of each experiment by a phenantroline-based spectrophotometric method according to the ISO 6332:1998 standard, after pre-filtration of the sample using a 0.22 µm nylon syringe-driven filter. Fe (II) forms a chelate complex with 1,10-phenanthroline. To measure the total iron in the sample, a spatula tip of ascorbic acid is also added to reduce Fe(III). The limit of quantification (LOQ) of this method was 0.25 mg/L, being the limit of detection (LOD) 0.1 mg/L.

2.5- Photodegradation reactions

The photodegradation experiments under solar radiation were conducted in a CPC pilot plant photoreactor operating at a tilt angle equal to the PSA latitude (37.09°N). The CPC photoreactor consists of two borosilicate tubes working in series and allowing for a 90 % transmission of the UV-A radiation from the natural solar spectrum. Each of the borosilicate tubes has a 5 cm internal diameter and a reflecting Al surface of 0.224 m^2 (length: 140.5 cm, width: 16.5 cm). The total volume was 10 L with a total illuminated volume of 1.9 L filled with cylinders of Ti-modified $LaFeO_3$/SiC alveolar foams (Figure 1). For details on the auxiliary facilities and the overall configuration of the experimental setup, the reader may refer to [29].

The 10 L contaminated water matrix was first homogenised by recirculation within the pilot plant at a water flow rate of 30 L/min in dark conditions for 30 min (CPC photoreactor covered), and a sample was subsequently taken to check the initial pollutant concentration, as well as the TOC concentration in the case of 4-CP. Afterwards, H_2O_2 or PS was added as oxidant, and the CPC photoreactor was further uncovered and exposed to sunlight. All the experiments were run in full sunshine for 4 h, and samples were taken at predetermined times. The UV-A irradiance during the degradation tests was 27–47 W/m^2, monitored with a global UV-A radiometer (KIPP& Zonnen, CUV4 model, 300–400 nm), located on a platform tilted at the same angle as the CPCs (37°).

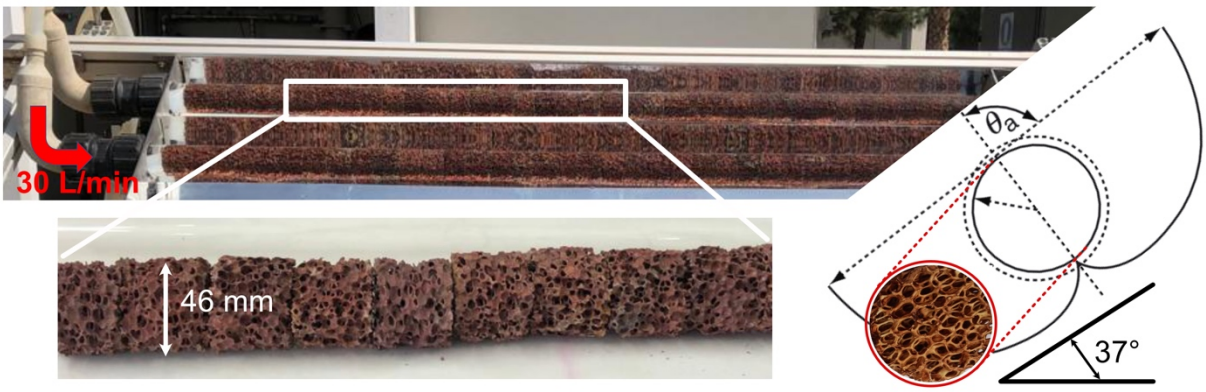

Figure 1. CPC photoreactor consisting in two borosilicate tubes operating in series and filled with cylinders of the Ti-modified $LaFeO_3$/SiC alveolar foam catalyst. Simplified schematic side-view of the CPC solar reactor.

The catalyst performances and the reaction kinetics were assessed by considering the accumulated solar UV energy per unit reactor volume collected by the reactor during the experiment (Q_{UV}, Eq. 1) rather than the experimental time. This allows a fair comparison among the different experimental runs by getting rid of the variations of the solar radiations. The experimental errors calculated from both the duplication of tests and the uncertainty in the analytical measurements were below 5%.

$$Q_{UV,n+1} = Q_{UV,n} + \Delta t_n UV_{G,n} \frac{A_i}{V_T} \qquad \text{[eq.1]}$$

where: Q_{UV} is the accumulated solar UV energy per unit of volume (kJ/L); $UV_{G,n}$ (W/m^2) is the average solar UV-A radiation measured between t_{n+1} and t_n (s); A_i is the irradiated (solar collector) area (m^2); V_T is the total volume of the plant (L).

3. RESULTS AND DISCUSSION

3.1. Catalyst characterization

Figure 2 shows the XRD pattern of the $La_{1-x}Ti_xFeO_3$/SiC foam catalyst. It shows the diffraction lines indexed to the Pbnm orthorhombic unit cell of $LaFeO_3$ (JCPDS card 070-7777). Beside the dominant reflexes assigned to the multiple SiC polytypes and to the alumina phase composing the ceramic foam support, diffraction lines indexed to the Pbnm orthorhombic unit cell of $LaFeO_3$ (JCPDS card 070-7777) were observed. In previous works conducted on Ti-substituted $LaFeO_3$ orthoferrite powders, complete structural refinement with cationic site occupation demonstrated the partial substitution of La by Ti within the $LaFeO_3$ matrix, and the significant change in the Pbnm orthorhombic unit cell parameters observed revealed consequently the insertion of Ti within the structure and the $La_{1-x}Ti_xFeO_3$ nature of the powders. The reflexes observed in the XRD pattern of the SiC foam supported catalyst confirmed the structural analogy between the $La_{1-x}Ti_xFeO_3$/SiC foam and the powdery $La_{1-x}Ti_xFeO_3$. For more details, the reader can refer to Garcia-Munoz et al. [28]. The optical images of both the bare SiC foam and the supported $La_{1-x}Ti_xFeO_3$-based catalysts show the macroscopic homogeneity of the coating on the SiC foam cylinders.

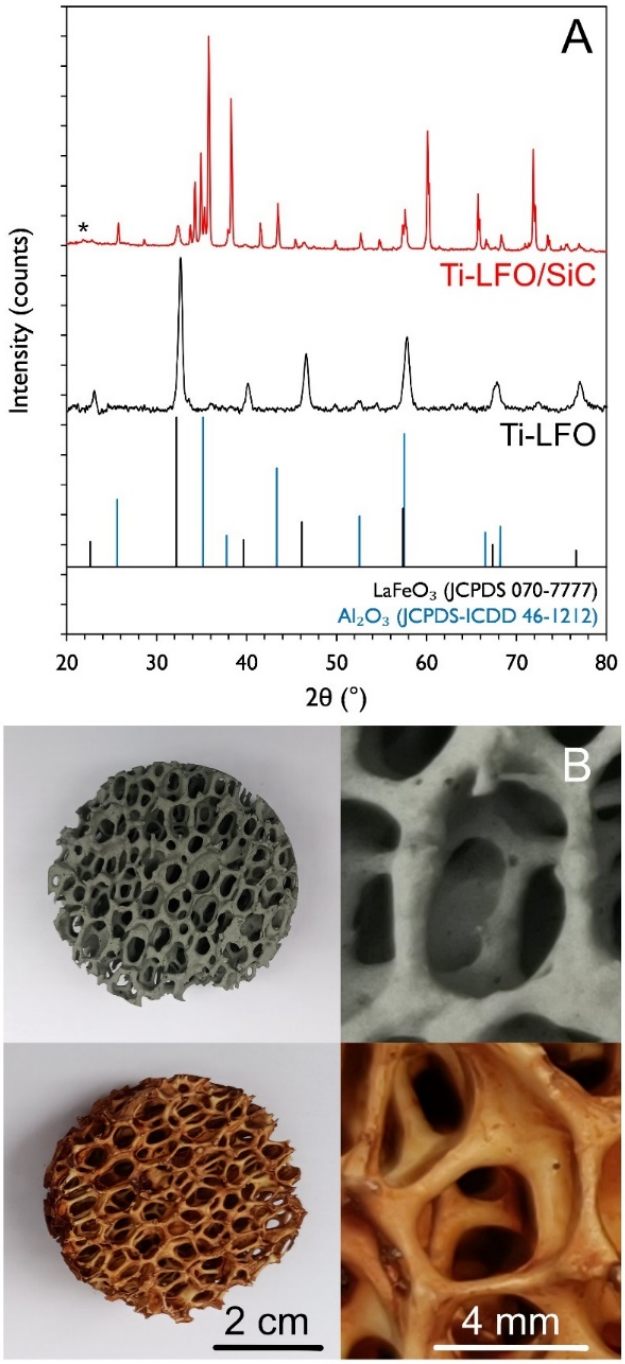

Figure 2. (A) XRD patterns of the $La_{1-x}Ti_xFeO_3$/SiC foam and the powdery $La_{1-x}Ti_xFeO_3$ counterpart. The intensity of the diffraction peaks corresponding to the supported $La_{1-x}Ti_xFeO_3$ phase has been necessarily amplified by scratching the surface of the $La_{1-x}Ti_xFeO_3$/SiC foam. This allowed for minimising the masking presence of the multiple reflexes corresponding to the largely dominant phases which come from the 3D ceramic foam support. The positions of the Bragg reflections are represented by vertical bars, in black for the reflections indexed in the

Pbnm orthorhombic unit cell of $LaFeO_3$ and in blue for those of the α-alumina phase (CPDS-ICDD 46-1212). In the pattern of the $La_{1-x}Ti_xFeO_3$/SiC foam, all the other high intensity reflexes correspond to the multiple α (4H and 6H) and β (3C) SiC polytypes, with hexagonal and cubic crystalline structures, respectively. The very small asterisk at ca. 2θ=22° corresponds to the silicon oxide phase impurity. **(B)** Optical images of the bare SiC foam support and the $La_{1-x}Ti_xFeO_3$/SiC foam.

3.2 Pilot-plant *vs.* lab-scale

Prior to the assessment of the capacity of the novel $La_{1-x}Ti_xFeO_3$/SiC foam catalyst to be used at the pilot-plant scale for the removal of MPs, preliminary tests were performed using 4-CP as model pollutant for evaluating its efficiency with a simple and well-known contaminant used for testing AOP light-driven catalysts during decades [30]. To this end, Figure 3 shows the evolution of both 4-CP and TOC concentrations along time, the experiments being carried out using the H_2O_2 dose theoretically needed for achieving a total mineralization of 20 mg/L of 4-CP, namely 125 mg/L. For the sake of comparison, Table 3 shows the main parameters of the photoreactions conducted at both lab and pilot-plant scales.

Table 3. Comparison of the main parameters of the photoreactions conducted at both lab and pilot-plant scale.

Parameters	**Lab scale** [a]	**Pilot-plant scale**
Volume to be treated	0.1 L	10 L
Catalyst	1 foam	37 foams
Amount of catalyst (mg)	50	1850
Reaction time (TOC removal)	120 min (>99%)	120 min (75%)
k'_{TOC} (mg/Lmin)	0.137	0.085
$k'_{4\text{-}CP}$ (min^{-1})	0.036	0.091

[a] Reaction parameters and data taken from the previous lab-scale studies of the authors [28].

The results obtained with the $La_{1-x}Ti_xFeO_3$/SiC foam catalyst showed that 75% TOC removal was achieved for an energy collected by the reactor of 13 kJ/L over a 120 min timescale, while a 4-CP removal below the quantification limit was already reached for an energy collected of 3kJ/L, that corresponded to 60 min of operation. H_2O_2 showed a total depletion within 120 min of reaction (data not shown). Remarkably, no iron leaching to the solution was detected along the photoreaction, so that the catalyst operated *via* pure heterogeneous surface reactions. This was in good agreement with the experiments carried out at the lab scale for which no iron leaching was observed, regardless of whether the tests were carried out with the $La_{1-x}Ti_xFeO_3$ catalyst as powdery material or supported on SiC foams, under UV-A or simulated solar light [5, 7, 28].

The experimental data were fitted following pseudo-first-order and pseudo-zero-order kinetic laws for the main pollutant and the TOC, respectively, as usual for photoassisted reactions. On the pilot-plant scale, apparent kinetic rate constants of 0.091 min^{-1} and 0.085 mg/Lmin were obtained for 4-CP degradation and mineralization, respectively. These values have to be put in perspective of the apparent kinetic rate constants for 4-CP degradation and mineralization obtained on the lab scale using the $La_{1-x}Ti_xFeO_3$/SiC foam catalyst in a batch-mode under 60 W m^{-2} of artificial UV-A irradiance, for treating a similar concentration of 4-CP, namely 0.036 min^{-1} and 0.137 mg/Lmin, respectively. At the lab scale, those values could be increased up to 0.06 min^{-1} and 0.3 mg/Lmin, respectively, when increasing the incident irradiance to 120 W m^{-2} [5-7, 28]. The faster degradation kinetics observed under solar radiation in the pilot system compared to the lab-scale test relies on better lighting of the foam cylinders due to the geometry of the solar photoreactor. However, the mineralisation was slower in the pilot system. This behaviour might result from the adsorption on the catalyst of the reaction

intermediates formed from 4-CP. Indeed, the pilot system is characterised by a lower amount of catalyst per unit of volume (and thus per mole of 4-CP degradation intermediates) compared to the lab-scale, namely 3.7 foams per litre *vs.* 10 foams per litre. The adsorption of the 4-CP degradation intermediates could reduce the catalyst efficiency and lower the mineralisation rate in the advanced stages of the degradation. This revealed the ability of the supported catalyst to operate in solar CPC photoreactors of several meters length under flow of water without high pressure drop. Secondly, the kinetics obtained are in the same range than those obtained during the lab scale studies.

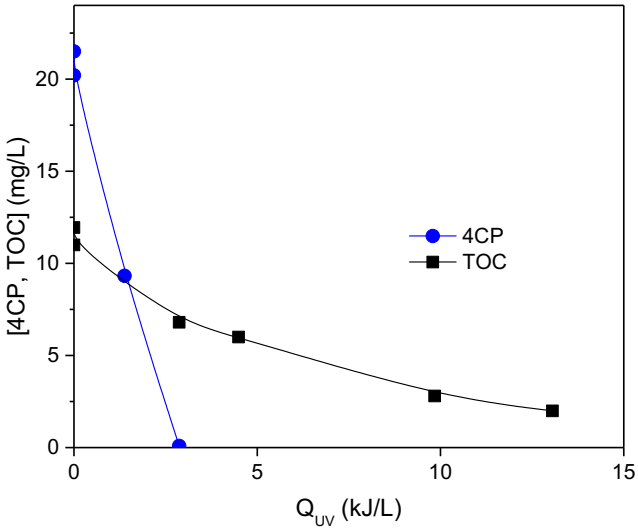

Figure 3. 4-CP oxidation and TOC mineralization in DW under solar light in the CPC photoreactor at the pilot-plant scale with the $La_{1-x}Ti_xFeO_3$/SiC foam catalyst. Operational conditions: $[4\text{-CP}]_0$= 20 mg/L, V_R= 10 L; circumneutral pH, $[H_2O_2]$ = 125 mg/L. Q_{UV} of 3 and 13 kJ/L were collected for test durations of 60 min and 120 min, respectively.

3.3 Photodegradation of micropollutants in demineralized water

The degradation of the imidacloprid (IMI) pesticide was assessed at a lower concentration, namely 1000 µg/L. The results obtained using 50 mg/L of H_2O_2 shown in Figure

4A depicted that a solar energy of 4.4 kJ/L was needed to reach the removal of IMI until quantification limit with an apparent kinetic rate constant k'_{imi}= 0.07 min^{-1}.

The ability of the catalyst to treat water was further assessed on a cocktail of five MPs (100 µg/L of each MP) normally detected at low concentrations after the secondary treatment of urban wastewater treatment plant, namely Caffeine, Trimethoprim, Sulfamethoxazole, Carbamazepine and Diclofenac (Figure 4B). The use of the micropollutant cocktail resulted in the increase to 30 KJ/L of the energy that the reactor needs to collect to achieve a significant reduction of the micropollutant concentrations, what in consequence prolonged the reaction time needed. However, all the micropollutants were substantially degraded under irradiation, albeit to different extents, and with a final H_2O_2 consumption of 73% for an initial concentration of 50 mg/L. For an energy of 30 KJ/L (that corresponded to a reaction time of 240 min), Diclofenac was the micropollutant which undergone the highest degradation rate with a removal of efficiency of 95%, while Sulfamethoxazole has been found as the most persistent compound with a removal efficiency of 46%. Intermediate degradation rates were observed for the other micropollutants, reaching 54%, 53% and 62% for Carbamazepine, Trimethoprim and Caffeine, respectively. This is in agreement with the work of Kowalska et al. [31]. They studied the degradation of a mix of almost the same MPs *via* homogeneous photo-Fenton at circumneutral pH and showed that Diclofenac and Trimethoprim were faster oxidized than Sulfamethoxazole and Caffeine, with higher degradation rates. The absence of any leached iron measured at the end of the reaction corroborated the stability of the catalyst.

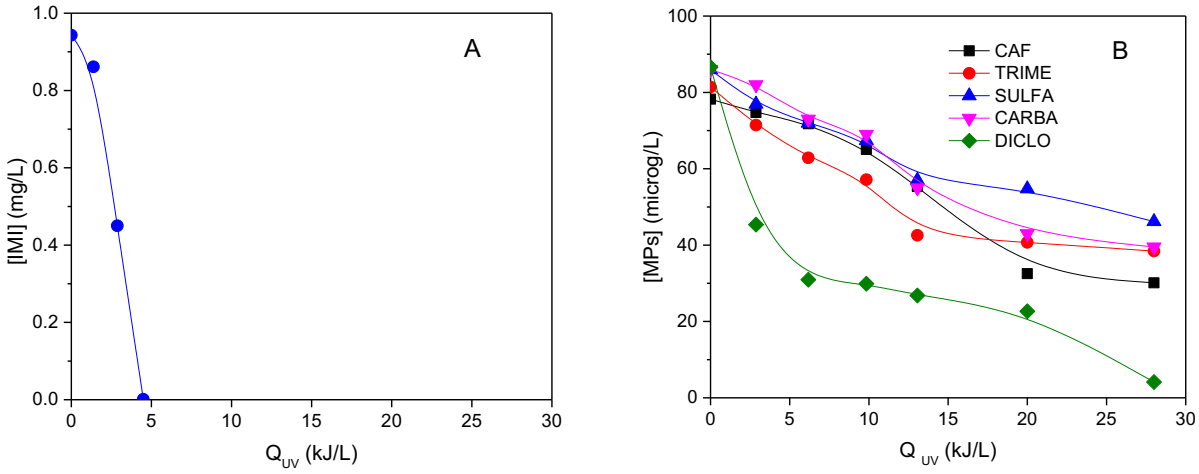

Figure 4. Performances obtained with the $La_{1-x}Ti_xFeO_3$/SiC foam catalyst in DW under solar light in the CPC photoreactor at the pilot-plant scale. **A)** IMI oxidation with $[IMI]_0$ = 1000 µg/L ; **B)** Oxidation of the mix of MPs, each of them at the initial concentration of 100 µg/L. Operational conditions in both cases: V_R= 10 L; circumneutral pH, $[H_2O_2]$ = 50 mg/L.

3.4. Effect of water matrices in the removal of pollutants

A step further in the assessment of the capacity of the $La_{1-x}Ti_xFeO_3$/SiC foam catalyst to treat water lies in its ability to adapt to a complex water matrix. The influence of the water matrix on the activity and stability of the $La_{1-x}Ti_xFeO_3$/SiC foam catalysts was studied first through the degradation of 4-CP at 20 mg/L in DW, TW and SUWW. The results shown in Figure 5 and Table 4 evidenced that the degradation and the mineralization of 4-CP are strongly impacted by the components of SUWW. This efficiency reduction was materialized by the extension of the treatment time with the increase in the water matrix complexity, from 30 min in DW to 180 min and 300 min in SUWWW and TW, respectively. In parallel, a decrease in the apparent reaction rate was observed, from 0.091 min^{-1} in DW down to 0.028 min^{-1} and 0.007 min^{-1} in SUWW and TW, respectively.

In terms of mineralization, it must be said that the TOC removal curves can only be compared for DW and TW due to the absence of extra-load of organic matter in both matrices. The mineralization rate decreased from 0.085 mg/Lmin to 0.015 mg/Lmin, which is indicative of a pronounced scavenger effect caused by the presence of salts in TW, that reduces drastically the overall activity of the catalyst. This effect has been observed previously in different works [32-34]. Although the matrix components are not directly involved in the surface mechanism that leads to the mineralization of the effluent, their competitive adsorption onto the catalyst surface impacts the apparent kinetic rate constants for the degradation of the main pollutant and that of the different intermediates. The matrix components also dramatically scavenge the produced oxidizing radicals [35].

After the tests, slightly lower pH values were measured at 3.8, 6.5 and 6.0 in DW, TP and SUWW, respectively, which resulted as usually from mineralization and short-chain organic acids formation. Independently of the water matrix complexity, no iron leaching from the catalyst to the solution was observed, suggesting a good stability of the catalytic material in operating conditions and consequently allowing for its consequent reuse. It is worth noting that the supported catalyst kept activity toward the main contaminant removal even in the presence of the different water components (Figure 5).

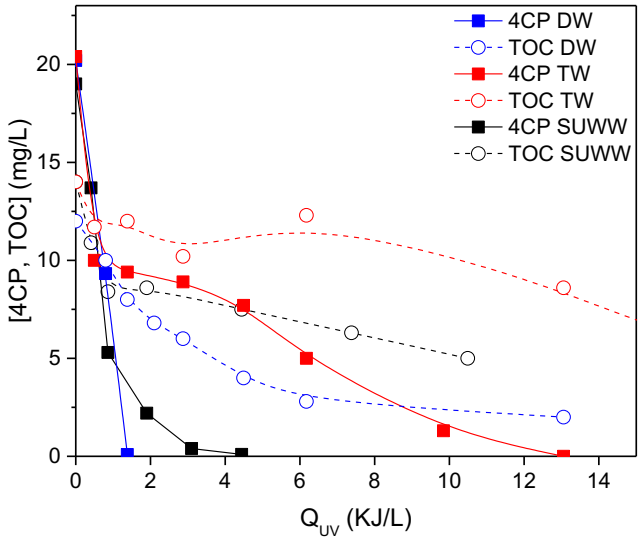

Figure 5. 4-CP oxidation and TOC mineralization with the $La_{1-x}Ti_xFeO_3$/SiC foam catalyst in different water matrices under solar light in the CPC photoreactor at the pilot-plant scale. Operational conditions: $[4\text{-CP}]_0$= 20 mg/L, $[TOC]_0$= 12 mg/L, V_R= 10 L; circumneutral pH, $[H_2O_2]$ = 125 mg/L. It must be said that $[TOC]_0$ in SUWW slightly exceeds the value of 12 mg/L due to the presence of organic matter in the aqueous matrix. 13-15 KJ/L corresponds to 120 min of photoreaction.

Table 4. Pseudo kinetic rate constants for the removal of 4-CP and TOC in different water matrices with the $La_{1-x}Ti_xFeO_3$/SiC foam catalyst under solar light in the CPC photoreactor at the pilot-plant scale (derived from Figure 5).

	DW	**TW**	**SUWW**
$k'_{4\text{-CP}}$ (min^{-1})	0.091	0.0065	0.0275
k'_{TOC} (mg/Lmin)	0.085	0.0150	0.0240

A step further in the assessment of the capacity of the $La_{1-x}Ti_xFeO_3$/SiC foam catalyst to treat water consisted in evaluating the effect of the water matrix on the removal of the mixture

of MPs in a more realistic µg/L concentration range as previously studied in DW. As can be inferred, the presence of salts and of organic components in the TW and SUWW matrices, respectively, resulted in a decrease in the oxidation rate of the different contaminants (Figure 6A-E). Figure 6F shows the impact of the different water matrices on the initial oxidation rate of the individual micropollutants. Whatever the targeted micropollutant, the removal rate decreased in TW and SUWW compared to DW, the effect being more pronounced in SUWW.

The extent to which the micropollutant degradation is affected by the water quality was shown to depend on its nature. In pure DW, the oxidation rates follow the order $k_{DICLO}>k_{CAF}>k_{CARB}>k_{TRIME}>k_{SULFA}$, that differs from that observed in both TW and SUWW (Figure 6). Indeed, tests in both TW and SUWW matrices evidenced that the rates of DICLO and CAF degradation were highly impacted by the water components, while those for TRIME, SULFA and CARBA were less affected (see rates in Table 5 and 6). However, it was worth noting that a significant decrease in the pollutant concentration was observed throughout the process in all the cases, the degradation percentages ranging from 62 to 95% for DW, 17 to 66% for TW and 8 to 42% for SUWW. CAF and DICLO were the micropollutants being the least and more affected by the treatment for ≈27-28 KJ/L, respectively (Table 6).

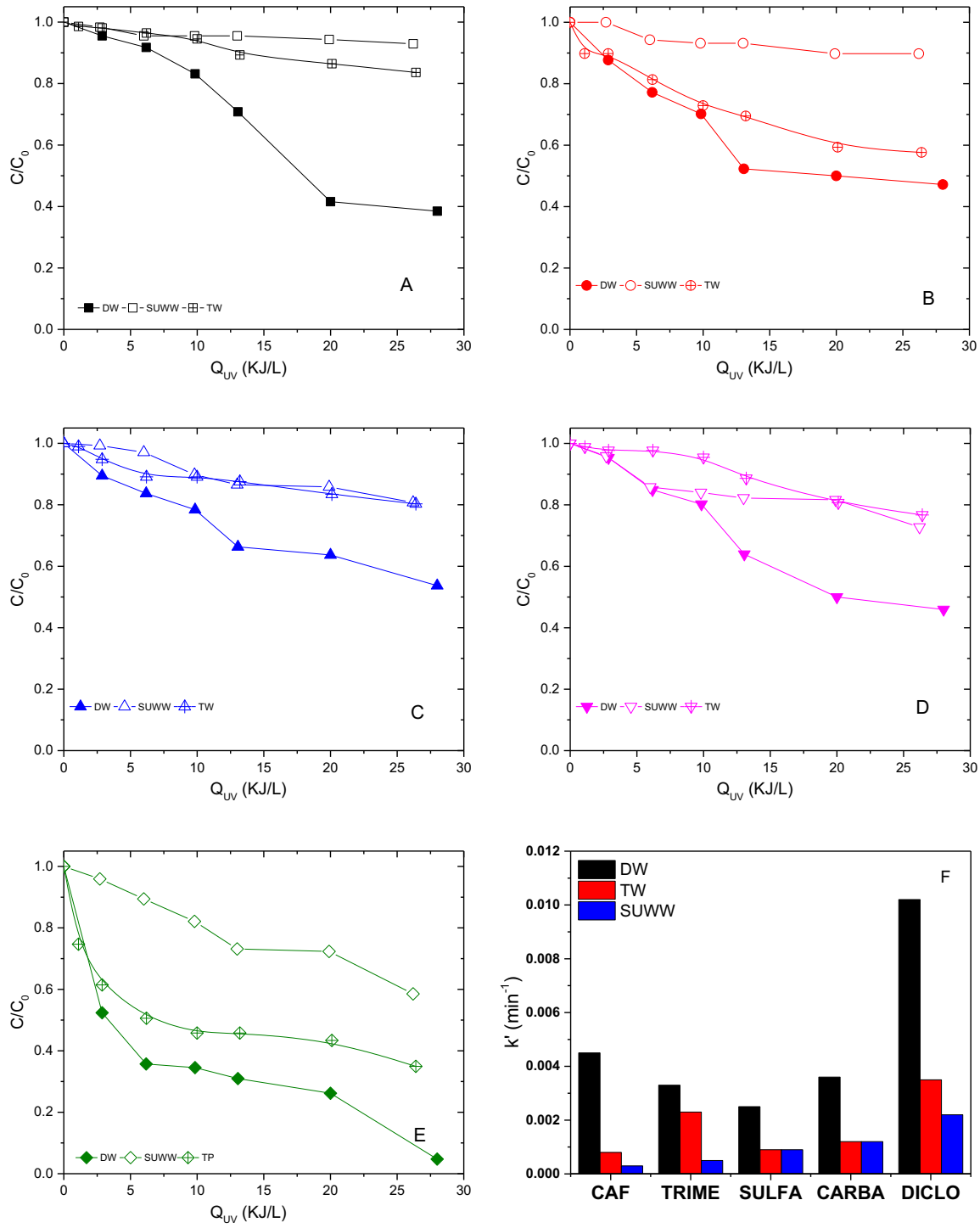

Figure 6. Oxidation of the mix of MPs in different water matrices with the $La_{1-x}Ti_xFeO_3$/SiC foam catalyst under solar light in the CPC photoreactor at the pilot-plant scale. A) CAF; B) TRIME; C) SULFA; D) CARBA; E) DICLO; F) Apparent initial reaction rates for the removal of MPs in different

water matrices. Operational conditions: V_R= 10 L; circumneutral pH, [H_2O_2] = 50 mg/L. The highest energy collected by the CPC reactor reported on the graphs for each experiment (*ca.* 27 KJ/L) corresponds to 240 min of reaction approximately. No change of pH values was observed due to the low MP concentration.

Table 5. Pseudo kinetic rate constants for the removal of MPs in the cocktail configuration in different water matrices with the $La_{1-x}Ti_xFeO_3$/SiC foam catalyst under solar light in the CPC photoreactor at the pilot-plant scale, as derived from Figs. 6A-E.

k' (min^{-1})	**DW**	**TW**	**SUWW**
k'_{CAF}	0.0045	0.0008	0.0003
k'_{TRIME}	0.0033	0.0023	0.0005
k'_{SULFA}	0.0025	0.0009	0.0009
k'_{CARBA}	0.0036	0.0012	0.0012
k'_{DICLO}	0.0102	0.0035	0.0022

Table 6. Influence of the water matrix on the conversion of MPs reached after 240 min of test (what corresponded to a solar radiation of *ca.* 27 KJ/L), as derived from Figs. 6A-E.

$X_{27\ KJ/L}$ (%)	**DW**	**TW**	**SUWW**
X_{CAF}	62	17	8
X_{TRIME}	53	43	11
X_{SULFA}	46	20	20
X_{CARBA}	54	24	28
X_{DICLO}	95	66	42

3.5. Effect of the water matrix in the removal of the micropollutants using $Na_2S_2O_8$ as oxidizing agent

In order to study the viability of the process for treating real effluents, the degradation process was also implemented in the MP cocktail configuration using sodium persulfate (PS) as oxidizing agent instead of H_2O_2, at the same concentration of oxidant (50 mg/L). The degradation curves obtained in the different water matrices are shown in Figure 7, and Table 7 compares the conversion of the pollutants achieved after 240 min using H_2O_2 and PS (corresponding to *ca.* 27 kJ/L of collected energy).

In DW, the order of magnitude of the MP removal was similar (apart from CARBA) regardless of whether H_2O_2 or PS was used, while the use of PS led to a higher efficiency in TW or SUWW whatever the pollutant targeted. In DW, larger removals of CAF and DICLO were observed with H_2O_2, while higher oxidation rates were obtained with PS for TRIME, CARBA and DICLO. In both TW and SUWW, the highest removal efficiencies were obtained with PS independently of the pollutant targeted.

The fact that the PS efficiency is less affected by the water composition must be related to its mechanism of reaction and its more selective nature, as both oxidants differ strongly in the nature of the oxidizing species they generate, namely $SO_4^{\bullet-}$ for PS and $HO^\bullet$ for H_2O_2. PS generates two $SO_4^{\bullet-}$ in the presence of light, while H_2O_2 only provides one $HO^\bullet$. In fact, it is known that the detrimental effect of chloride, sulfates and carbonates (which are scavengers of $HO^\bullet$ [36]) is lower with PS than with H_2O_2, what is of prime importance as both TW and SUWW contain those anions in large concentrations. It can also be noticed that both $HO^\bullet$ and $SO_4^{\bullet-}$ radicals strongly differ in terms of their action mode. $SO_4^{\bullet-}$ acts better at circumneutral pH as its redox potential (1.8–2.7 V) is higher than the one of $HO^\bullet$ [37]. Besides, $SO_4^{\bullet-}$ presents a longer lifetime (30-40 µs) compared to $HO^\bullet$ (<1 µs) [38]. On the other hand, $SO_4^{\bullet-}$ is

characterized by its selective nature compared to $HO^{\bullet}$[3]. While $SO_4^{\bullet-}$ attacks selectively -OH and $-NH_2$ groups present for instance in both CARBA and DICLO micropollutants, $HO^{\bullet}$ reacts unselectively with any chemical compounds from the water matrix, including unfortunately salts and organic matter [3]. This could explain the substantial oxidation of CARBA and DICLO regardless of the water matrix complexity when using PS as oxidant instead of H_2O_2. For this reason, PS is recently gaining interest as alternative oxidant to H_2O_2 [39-41].

Table 7. Conversion of MPs in different water matrices at *ca.* 27 kJ/L of collected energy (corresponding to 240 min of test), as derived from Figs. 7A-E.

Pollutant	DW		TW		SUW	
	H_2O_2	PS	H_2O_2	PS	H_2O_2	PS
CAF	62	27	17	21	8	44
TRIME	53	57	43	61	11	46
SULFA	46	31	20	27	20	53
CARBA	54	>99	24	>99	28	>99
DICLO	95	>99	66	>99	42	>99

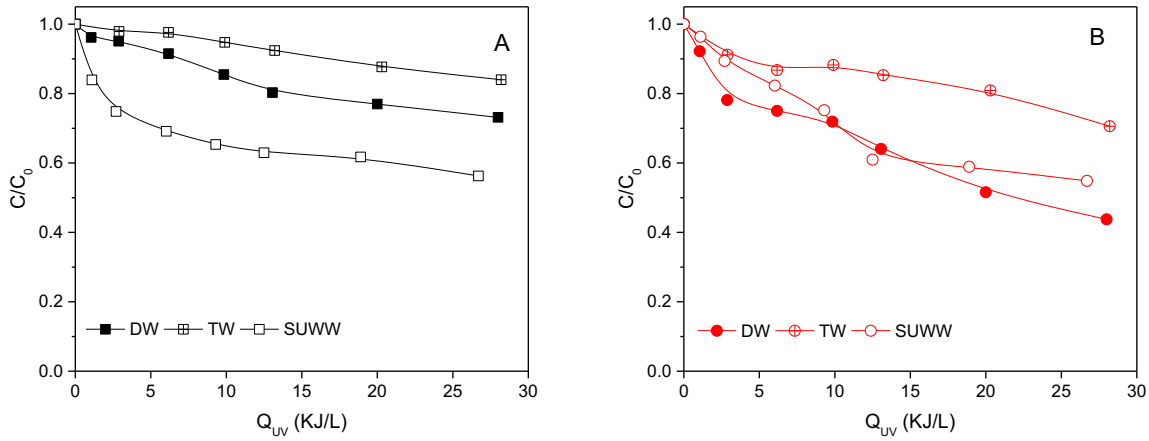

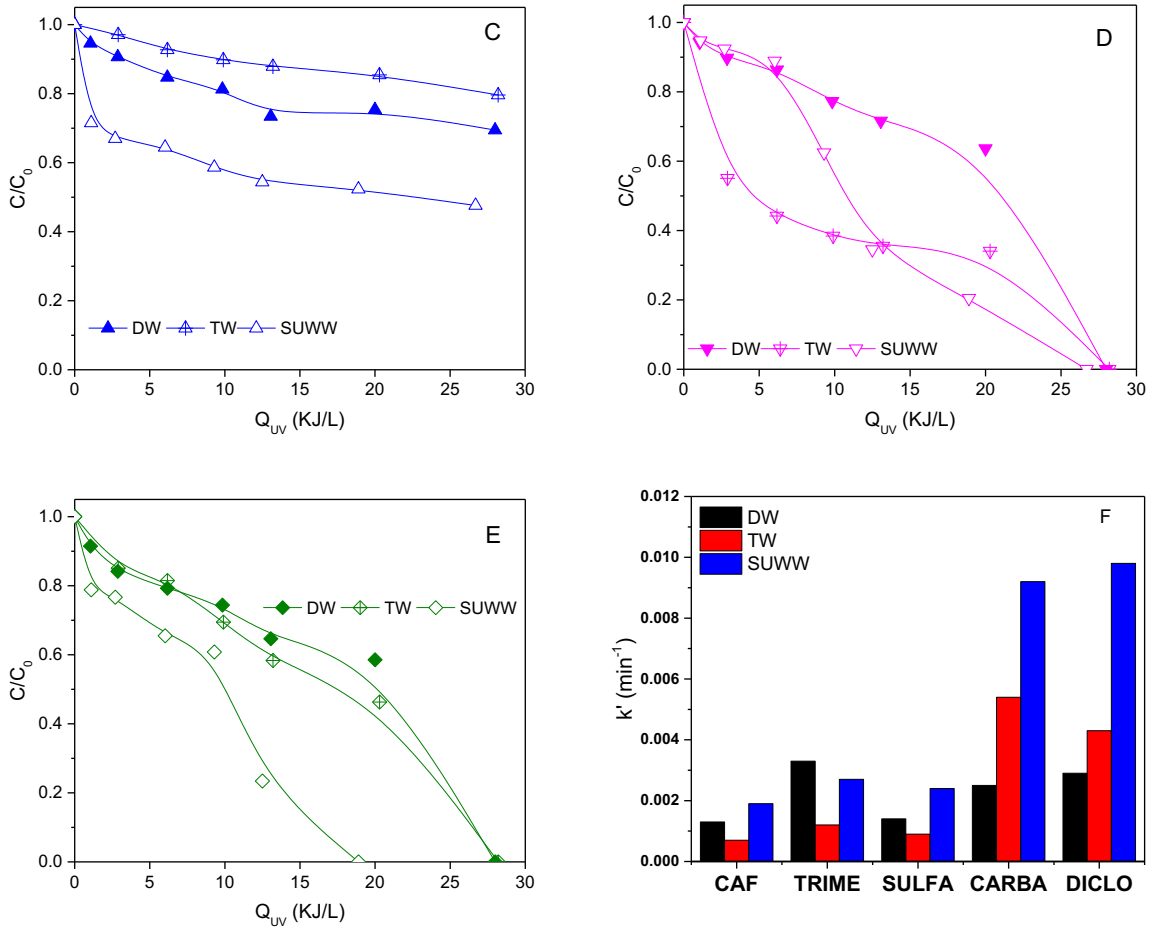

Figure 7. Oxidation of the mix of MPs in different water matrices with the $La_{1-x}Ti_xFeO_3$/SiC foam catalyst under solar light and using PS as oxidant in the CPC photoreactor. A) CAF; B) TRIME; C) SULFA; D) CARBA; E) DICLO; F) Apparent initial rate constants of the MP degradation in the different water matrices. Operational conditions: V_R= 10 L; circumneutral pH, [PS] = 50 mg/L. 240 min of test corresponded to *ca.* 27 kJ/L of collected energy.

Attending to results presented in Figure 7 (PS was more efficient than H_2O_2), treatment capacity of SUWW of the $La_{1-x}Ti_xFeO_3$/SiC foam catalyst could be roughly calculated taking into account treatment time (240 min, i.e. 26.7 KJ/L) system volume (10 L), solar collector area (0.224 m^2) and % of degradation (70%) of the mixture of MPs at 500 µg/L: 3800 µg m^{-2} h^{-1} at an average solar UV 45 W m^{-2}. Taking into account average solar UV in many sunny countries is around 20

W m^{-2}, average treatment capacity would be around 1700 µg m^{-2} h^{-1}, which means that 7.4 g m^{-2} $year^{-1}$ could be removed. MPs concentration in effluents from municipal treatment plants range between 0.050-0.100 g m^{-3} and the objective of advanced treatment would be 80% removal [1-4]. Therefore, the treatment capacity of the $La_{1-x}Ti_xFeO_3$/SiC foam catalyst (operated under the sun 4380 h per year) could be envisaged in the range of 150-75 m^3 m^{-2} $year^{-1}$.

Treatment capacity could be compared with other results available in the literature, for homogeneous photo-Fenton at circumneutral pH using iron complexes with PS (or H_2O_2), applied also to MPs in SUWW or real effluents at lab scale. For example, Cabrera-Reina et al. [3] with Fe-EDDS and PS got average treatment capacity around 60000 µg m^{-2} h^{-1} at 30 W m^{-2}, which accounts for 40000 µg m^{-2} h^{-1} at 20 W m^{-2}, clearly higher than $La_{1-x}Ti_xFeO_3$/SiC foam catalyst.

Ricardo et al. with Fe-NTA and PS get average treatment capacity around 5100 µg m^{-2} h^{-1} at 30 W m^{-2}, which accounts for 3400 µg m^{-2} h^{-1} at 20 W m^{-2} [42]. Gualda-Alonso et al. [43] presented a continuous flow solar demonstration plant of large size (100 m^2 raceway pond reactor) operating with Fe-NTA and H_2O_2 at circumneutral pH giving a treatment capacity of 0.80 m^3 m^{-2} d^{-1} at 25 W m^{-2}, eliminating 50% of 68 µg/L MPs. It accounts for 2300 µg m^{-2} h^{-1}. These two last examples using Fe-NTA gave results in the same range than $La_{1-x}Ti_xFeO_3$/SiC foam catalyst.

3.6 Long-term stability of the catalytic foams

All the former experiments were performed with the same $La_{1-x}Ti_xFeO_3$/SiC foam catalyst, so that the supported catalyst was used for more than 100 h under real solar light. Besides, the

durability of the material was challenged by performing at regular time-interval (every 20 h of use) a control reaction that consisted in degrading 4-CP at 20 mg/L in DW (reaction shown in Figure 3). In all cases, 75% of TOC mineralization was achieved after 13-15 kJ/L of energy collected, indicating that the activity of the catalyst was not affected by the large amount of experiments conducted over prolonged operation times under different conditions and in water matrices of different complexity. In all cases, no iron leaching was detected. However, this is not incompatible with a slow leaching of some of the supported nanomaterial. Long-lasting tests with specific analysis to assess whether nanomaterial leaching occurs, are currently underway.

4. CONCLUSIONS

The employment of a macroscopic photo-CWPO $La_{1-x}Ti_xFeO_3$/SiC alveolar foam catalyst has been scaled up for the first time within a CPC photoreactor operating under natural solar light for the efficient removal of model contaminants and different emerging organic micropollutants in wastewater matrices of different complexity using H_2O_2 and PS as oxidizing agent. No iron leaching, substantial degradation and mineralisation as well as long-time use, has not been described yet under so different and realistic conditions for any other macroscopic catalyst. The experiments showed that the $La_{1-x}Ti_xFeO_3$/SiC alveolar foam catalyst is efficient and stable for the removal of 4-CP, IMI and a mix of MPs at different concentration levels.

The reactions performed with H_2O_2 in DW revealed the need of increasing the collected energy when the concentration of the pollutant was decreased from the mg/L to the µg/L range, namely from *ca.* 4 KJ/L to *ca.* 27KJ/L. The composition of both TW and SUWW matrices highly affected the catalyst activity and the efficiency of the overall process, and independently

of the targeted micropollutant, the removal rate decreased in TW and SUWW compared to DW. In the case of MPs in the cocktail configuration, the slowing down effect was more pronounced in SUWW.

The use of PS as oxidant instead of H_2O_2 resulted in a better efficiency in the MP removal in DW and in some cases even better degradation rates were obtained when performing the oxidation reaction in TW and in SUWW. This can be related to the different reaction mechanism taking place when using PS rather than H_2O_2 and to the more selective nature of the $SO_4^{\bullet-}$ radicals generated under light, that allows the radicals and consequently the catalytic photodegradation process to be less affected by the presence of ions and organic matter in the water matrix. Nevertheless, although the use of PS is globally advantageous over H_2O_2, the efficiency of each oxidant upon the process remains strongly affected by the water matrix. Finally, while the absence of any detectable iron leaching to the solution was demonstrated regardless of the oxidant use and of the wastewater complexity, however, this is not incompatible with a slow long-term leaching of part of the supported nanoparticles, which needs to be further studied in detail.

The degradation performances combined to the stability of the catalyst indicate the prospect nature of the $La_{1-x}Ti_xFeO_3$/SiC alveolar foam catalysts to operate in a continuous way for the polishing effluents from a secondary wastewater treatment plant. Indeed, attending to the slower kinetics compared to other homogeneous photocatalysts, the simplicity of operation of the $La_{1-x}Ti_xFeO_3$/SiC foam catalyst would be a clear asset especially interesting for this application niche where volumes as high as millions of cubic metres per day are disposed. It is interesting to note the treatment capacity of 150-75 $m^3\ m^{-2}\ year^{-1}$ for eliminating 80% of MPs in municipal effluents containing 50-100 µg/L.

To this end, it is not necessary to use powerful systems, but rather to implement systems that are simple to operate. However, prolonged long-term testing with real effluents is still needed to get economical and operational key parameters.

CREDIT AUTHORSHIP CONTRIBUTION STATEMENT

P. García-Muñoz: Conceptualization, Data curation, Formal analysis, Funding acquisition, Methodology, Project administration, Supervision, Writing – review & editing, Resources. **A. Abega:** Investigation. **A. Hernández-Zanoletty**: Investigation, Supervision, Writing – review & editing. **S. Malato:** Data curation, Formal analysis, Investigation, Writing – review & editing. **D. Robert:** Investigation, Methodology, Funding acquisition. **N.Keller:** Formal Analysis, Funding acquisition, Methodology, Project administration, Resources, Supervision, Writing – original draft, Writing – review & editing.

CONFLICT OF INTEREST

The authors declare no conflict of interest.

ACKNOWLEDGEMENTS

P.G.M. acknowledges Comunidad de Madrid through the call Research Grants for Young Investigators from Universidad Politécnica de Madrid for funding the research project SUNCAT4PLAST (APOYO-JOVENES-21-JV4DEB-3-Q2WGKV). The authors acknowledge the Sfera III-823802-H2020-Transnational Access Program for the research stays of P.G.M. and A.A. at PSA. The authors wish to thank the Grant PID2021-126400OB-C33 (AquaEnAgri) funded by MCIN/AEI/ 10.13039/501100011033 and, by “ERDF A way of making Europe”. This work has

received financial support from Spanish MCIN/AEI/ 10.13039/501100011033 and “ERDF A way of making Europe”, through project PHOTORAS (PID2021-128165OA-I00).

REFERENCES

1. V. Geissen, H. Mol, E. Klumpp, G. Umlauf, M. Nadal, M. van der Ploeg, van de Zee, Sjoerd E. A. T. M., C.J. Ritsema, Emerging pollutants in the environment: A challenge for water resource management, International Soil and Water Conservation Research 3 (2015) 57-65.

2. A.R. Ribeiro, O.C. Nunes, M.F.R. Pereira, A.M.T. Silva, An overview on the advanced oxidation processes applied for the treatment of water pollutants defined in the recently launched Directive 2013/39/EU, Environ. Int. 75 (2015) 33-51.

3. A. Cabrera-Reina, M. Aliste, M.I. Polo-López, S. Malato, I. Oller, Individual and combined effect of ions species and organic matter on the removal of microcontaminants by Fe3+-EDDS/solar-light activated persulfate, Water Res. 230 (2023) 119566.

4. L. Rizzo, S. Malato, D. Antakyali, V.G. Beretsou, M.B. Đolić, W. Gernjak, E. Heath, I. Ivancev-Tumbas, P. Karaolia, A.R. Lado Ribeiro, G. Mascolo, C.S. McArdell, H. Schaar, A.M.T. Silva, D. Fatta-Kassinos, Consolidated vs new advanced treatment methods for the removal of contaminants of emerging concern from urban wastewater, Sci. Total Environ. 655 (2019) 986-1008.

5. P. Garcia-Muñoz, C. Lefevre, D. Robert, N. Keller, Ti-substituted LaFeO3 perovskite as photoassisted CWPO catalyst for water treatment, Applied Catalysis B: Environmental 248 (2019) 120-128.

6. P. García-Muñoz, F. Fresno, C. Lefevre, D. Robert, N. Keller, Synergy Effect Between Photocatalysis and Heterogeneous PhotoFenton Catalysis on Ti-Doped LaFeO3 Perovskite for High Efficiency Light-Assisted Water Treatment, Catal. Sci. Technol. (2020).

7. P. Garcia-Muñoz, F. Fresno, C. Lefevre, D. Robert, N. Keller, Highly robust La1-xTixFeO3 dual catalyst with combined photocatalytic and photo-CWPO activity under visible light for 4-chlorophenol removal in water, Applied Catalysis B: Environmental 262 (2020) 118310.

8. P. García-Muñoz, G. Pliego, J.A. Zazo, J.A. Casas, PHOTOCATALYTIC WET PEROXIDE OXIDATION PROCESS AT CIRCUMNEUTRAL pH USING ILMENITE AS CATALYST, Journal of Environmental Chemical Engineering (2018).

9. J.A. Rengifo-Herrera, C. Pulgarin, Why five decades of massive research on heterogeneous photocatalysis, especially on TiO2, has not yet driven to water disinfection and detoxification applications? Critical review of drawbacks and challenges, Chem. Eng. J. 477 (2023) 146875.

10. D. Robert, V. Keller, N. Keller, Pichat P. (Ed), Photocatalysis and Water Purification: From Fundamentals to Recent Applications, Wiley-VCH, Weinheim, 2013.

11. M.M. Hossain, G.B. Raupp, S.O. Hay, T.N. Obee, Three-dimensional developing flow model for photocatalytic monolith reactors, AIChE J. 45 (1999) 1309-1321.

12. J. Taranto, D. Frochot, P. Pichat, Photocatalytic air purification: Comparative efficacy and pressure drop of a TiO2-coated thin mesh and a honeycomb monolith at high air velocities using a 0.4m3 close-loop reactor, Separation and Purification Technology 67 (2009) 187-193.

13. P. Du, J.T. Carneiro, J.A. Moulijn, G. Mul, A novel photocatalytic monolith reactor for multiphase heterogeneous photocatalysis, Applied Catalysis A: General 334 (2008) 119-128.

14. P. Ávila, B. Sánchez, A.I. Cardona, M. Rebollar, R. Candal, Influence of the methods of TiO2 incorporation in monolithic catalysts for the photocatalytic destruction of chlorinated hydrocarbons in gas phase, Catalysis Today 76 (2002) 271-278.

15. Z. Warren, T. Tasso Guaraldo, A.S. Martins, J. Wenk, D. Mattia, Photocatalytic foams for water treatment: A systematic review and meta-analysis, Journal of Environmental Chemical Engineering 11 (2023) 109238.

16. G. Plantard, V. Goetz, Correlations between optical, specific surface and photocatalytic properties of media integrated in a photo-reactor, Chem. Eng. J. 252 (2014) 194-201.

17. K. Elatmani, N.B. oujji, G. Plantara, V. Goetz, I.A. ichou, 3D Photocatalytic media for decontamination of water from pesticides, Mater. Res. Bull. 101 (2018) 6-11.

18. C.B.D. Marien, M. Le Pivert, A. Azaïs, I.C. M'Bra, P. Drogui, A. Dirany, D. Robert, Kinetics and mechanism of Paraquat's degradation: UV-C photolysis vs UV-C photocatalysis with TiO2/SiC foams, J. Hazard. Mater. 370 (2019) 164-171.

19. I.J. Ochuma, O.O. Osibo, R.P. Fishwick, S. Pollington, A. Wagland, J. Wood, J.M. Winterbottom, Three-phase photocatalysis using suspended titania and titania supported on a reticulated foam monolith for water purification, Catalysis Today 128 (2007) 100-107.

20. M. Vargová, G. Plesch, U.F. Vogt, M. Zahoran, M. Gorbár, K. Jesenák, TiO2 thick films supported on reticulated macroporous Al2O3 foams and their photoactivity in phenol mineralization, Appl. Surf. Sci. 257 (2011) 4678-4684.

21. C.B.D. Marien, M. Le Pivert, A. Azaïs, I.C. M'Bra, P. Drogui, A. Dirany, D. Robert, Kinetics and mechanism of Paraquat's degradation: UV-C photolysis vs UV-C photocatalysis with TiO2/SiC foams, Journal of Hazardous Materials (2018).

22. T.M. Do, J.Y. Byun, S.H. Kim, Magnetite-coated metal foams as one-body catalysts for Fenton-like reactions, Research on Chemical Intermediates 43 (2017) 3481-3492.

23. S. Li, G. Zhang, H. Zheng, Y. Zheng, P. Wang, Application of BiFeO3-based on nickel foam composites with a highly efficient catalytic activity and easily recyclable in Fenton-like process under microwave irradiation, J. Power Sources 386 (2018) 21-27.

24. X. Ou, F. Pilitsis, Y. Jiao, Y. Zhang, S. Xu, M. Jennings, Y. Yang, S.F.R. Taylor, A. Garforth, H. Zhang, C. Hardacre, Y. Yan, X. Fan, Hierarchical Fe-ZSM-5/SiC foam catalyst as the foam bed catalytic reactor (FBCR) for catalytic wet peroxide oxidation (CWPO), Chem. Eng. J. 362 (2019) 53-62.

25. X. Ou, F. Pilitsis, N. Xu, S.F.R. Taylor, J. Warren, A. Garforth, J. Zhang, C. Hardacre, Y. Jiao, X. Fan, On developing ferrisilicate catalysts supported on silicon carbide (SiC) foam catalysts for continuous catalytic wet peroxide oxidation (CWPO) reactions, Catalysis Today 356 (2020) 631-640.

26. C. Orak, S. Atalay, G. Ersöz, Photocatalytic and photo-Fenton-like degradation of methylparaben on monolith-supported perovskite-type catalysts, Sep. Sci. Technol. 52 (2017) 1310-1320.

27. P. Abdi, A. Farzi, A. Karimi, Application of a hybrid enzymatic and photo-fenton process for investigation of azo dye decolorization on TiO2/metal-foam catalyst, Journal of the Taiwan Institute of Chemical Engineers 71 (2017) 137-144.

28. P. García-Muñoz, F. Fresno, C. Lefevre, D. Robert, N. Keller, Ti-Modified LaFeO3/β-SiC Alveolar Foams as Immobilized Dual Catalysts with Combined Photo-Fenton and Photocatalytic Activity, ACS Appl. Mater. Interfaces 12 (2020) 57025-57037.

29. M.H. Pérez, G. Peñuela, M.I. Maldonado, O. Malato, P. Fernández-Ibáñez, I. Oller, W. Gernjak, S. Malato, Degradation of pesticides in water using solar advanced oxidation processes, Applied Catalysis B: Environmental 64 (2006) 272-281.

30. H. Al-Ekabi, N. Serpone, E. Pelizzetti, C. Minero, M.A. Fox, R.B. Draper, Kinetic studies in heterogeneous photocatalysis. 2. Titania-mediated degradation of 4-chlorophenol alone and in a three-component mixture of 4-chlorophenol, 2,4-dichlorophenol, and 2,4,5-trichlorophenol in air-equilibrated aqueous media, Langmuir 5 (1989) 250-255.

31. K. Kowalska, M. Roccamante, A. Cabrera Reina, P. Plaza-Bolaños, I. Oller, S. Malato, Pilot-scale removal of microcontaminants by solar-driven photo-Fenton in treated municipal effluents: Selection of operating variables based on lab-scale experiments, Journal of Environmental Chemical Engineering 9 (2021) 104788.

32. P. Garcia-Muñoz, W. Dachtler, B. Altmayer, R. Schulz, D. Robert, F. Seitz, R. Rosenfeldt, N. Keller, Reaction pathways, kinetics and toxicity assessment during the photocatalytic degradation of glyphosate and myclobutanil pesticides: Influence of the aqueous matrix, Chemical Engineering Journal 384 (2020) 123315.

33. J. Carbajo, P. García-Muñoz, A. Tolosana-Moranchel, M. Faraldos, A. Bahamonde, Effect of water composition on the photocatalytic removal of pesticides with different TiO2 catalysts, Environmental Science and Pollution Research (2014).

34. A.R. Lado Ribeiro, N.F.F. Moreira, G. Li Puma, A.M.T. Silva, Impact of water matrix on the removal of micropollutants by advanced oxidation technologies, Chem. Eng. J. 363 (2019) 155-173.

35. Y. Zhang, Y. Zhao, F. Maqbool, Y. Hu, Removal of antibiotics pollutants in wastewater by UV-based advanced oxidation processes: Influence of water matrix components, processes optimization and application: A review, Journal of Water Process Engineering 45 (2022) 102496.

36. E. Grilla, V. Matthaiou, Z. Frontistis, I. Oller, I. Polo, S. Malato, D. Mantzavinos, Degradation of antibiotic trimethoprim by the combined action of sunlight, TiO2 and persulfate: A pilot plant study, Catalysis Today 328 (2019) 216-222.

37. W. Oh, Z. Dong, T. Lim, Generation of sulfate radical through heterogeneous catalysis for organic contaminants removal: Current development, challenges and prospects, Applied Catalysis B: Environmental 194 (2016) 169-201.

38. T. Olmez-Hanci, I. Arslan-Alaton, Comparison of sulfate and hydroxyl radical based advanced oxidation of phenol, Chem. Eng. J. 224 (2013) 10-16.

39. L. Li, Y. Deng, J. Ai, L. Li, G. Liao, S. Xu, D. Wang, W. Zhang, Fe/Mn loaded sludge-based carbon materials catalyzed oxidation for antibiotic degradation: Persulfate vs H2O2 as oxidant, Separation and Purification Technology 263 (2021) 118409.

40. S. Guerra-Rodríguez, E. Rodríguez, J. Moreno-Andrés, J. Rodríguez-Chueca, Effect of the water matrix and reactor configuration on Enterococcus sp. inactivation by UV-A activated PMS or H2O2, Journal of Water Process Engineering 47 (2022) 102740.

41. S. Giannakis, S. Samoili, J. Rodríguez-Chueca, A meta-analysis of the scientific literature on (photo)Fenton and persulfate advanced oxidation processes: Where do we stand and where are we heading to?, Current Opinion in Green and Sustainable Chemistry 29 (2021) 100456.

42. I.A. Ricardo, E.O. Marson, C.E.S. Paniagua, D.L.P. Macuvele, Starling, Maria Clara V. M., J.A.S. Pérez, A.G. Trovó, Microcontaminants degradation in tertiary effluent by modified solar photo-Fenton process at neutral pH using organic iron complexes: Influence of the peroxide source and matrix composition, Chem. Eng. J. 487 (2024) 150505.

43. E. Gualda-Alonso, N. Pichel, P. Soriano-Molina, E. Olivares-Ligero, F.X. Cadena-Aponte, A. Agüera, J.A. Sánchez Pérez, J.L. Casas López, Continuous solar photo-Fenton for wastewater reclamation in operational environment at demonstration scale, J. Hazard. Mater. 459 (2023) 132101.